

# The Fifth UltraVISTA Data Release

A. Moneti, H. J. McCracken, S. Rouberol,  
(Institut d’Astrophysique de Paris);  
J. Dunlop, M. Franx, J. Fynbo, R. Bowler, B. Milvang-Jensen (UltraVISTA);  
C. Gonzalez-Fernandez, E. Gonzalez-Solares, M. Irwin (CASU);  
R. Blake, N. Cross, R. Mann, M. Read, E. Sutorius (WFAU).

May 2, 2023

**Data Collection:** UltraVISTA  
**Release number** 5  
**Data provider:** Jim Dunlop  
**Date:** May 2, 2023

## 1 Abstract

UltraVISTA is an ultra-deep near-infrared survey of the central  $1.5^\circ \times 1.2^\circ$  region of the COSMOS field (Scoville et al. 2007). This document describes the fifth UltraVISTA data release, “DR5”, which comprises stacked images and catalogues in  $YJHK_s$  and the NB118 narrow-band filter. This release is based on data taken from 2009 to mid 2019, which is three observing seasons (years) more than DR4. The additional data have almost homogenised the exposure time in the “deep” and “ultra-deep” stripes in the  $J$ ,  $H$  and  $K_s$  filters, which now reach the same depths to  $\sim 0.15$  mag.

### 1.1 Acknowledging these data products

Any publications using these data products must include this text:

**“Based on observations collected at the European Southern Observatory under ESO programmes 179.A-2005 and 198.A-2003 and on data obtained from the ESO Science Archive Facility with DOI <https://doi.org/10.18727/archive/52>, and on data products produced by CALET and the Cambridge Astronomy Survey Unit on behalf of the UltraVISTA consortium.”** In addition, a reference to the UltraVISTA DR1 survey paper should be included: McCracken et al. (2012).

## 2 Overview

The DR5 release was built from the UltraVISTA data (from ESO programmes 179.A-2005 and 198.A-2003) obtained between 4 December 2009 and 2 May 2019, or ten observing seasons. The additional data since DR4 were obtained beginning on 6 November 2016 and were primarily at the “deep” stripes in  $J$  and  $H$ , and to a lesser extent at  $K_s$ , in order to bring those parts of the final stack to roughly the same depth as the “ultra-deep” stripes.

Our starting point are the data pre-processed by CASU (“Cambridge Astronomy Survey Unit”<sup>1</sup>), who performed dark subtraction, flat-fielding, non-linearity correction, gain normalisation, and an initial sky subtraction (e.g. Irwin et al. 2004; Lewis et al. 2010, and the CASU web site<sup>2</sup>). A total of 91,731 individual images and their ancillary files (flat fields, sky frames, stacks) were downloaded from the CASU web site and processed as described below. Of these 81,125 images passed our selection criteria (mainly on PSF FWHM and ellipticity, cf. Fig. 1) and were used to produce the stacks in the five filters<sup>3</sup>.

The main purpose of our reprocessing is to improve on the sky subtraction, as will be described below. The processing pipeline differs slightly from the one used in DR4: (1) an additional selection criterion is used to identify files with unusual effects, (2) the rejection of files is done at a later stage so that rejected files are still used for the sky determination, and (3) the “global” object mask, used to produce individual masks to avoid faint sources in building the individual skies, was built from the DR4 stacks rather than from a preliminary stack built from the CASU files. Furthermore, the Gaia EDR3 reference catalogue (Gaia Collaboration et al. 2016, 2021; Lindegren et al. 2021) is used for the astrometric correction, and updated versions of the Astromatic codes are used in the processing.

Figure 1 shows the seeing and ellipticity distributions, measured using PSFEx (Bertin 2011), of all the images, separated by filter. The red solid line represents the mode of each distribution, and the blue dashed line shows the cut-off thresholds adopted. In general, the median values in each filter are very similar as a consequence of queue scheduling.

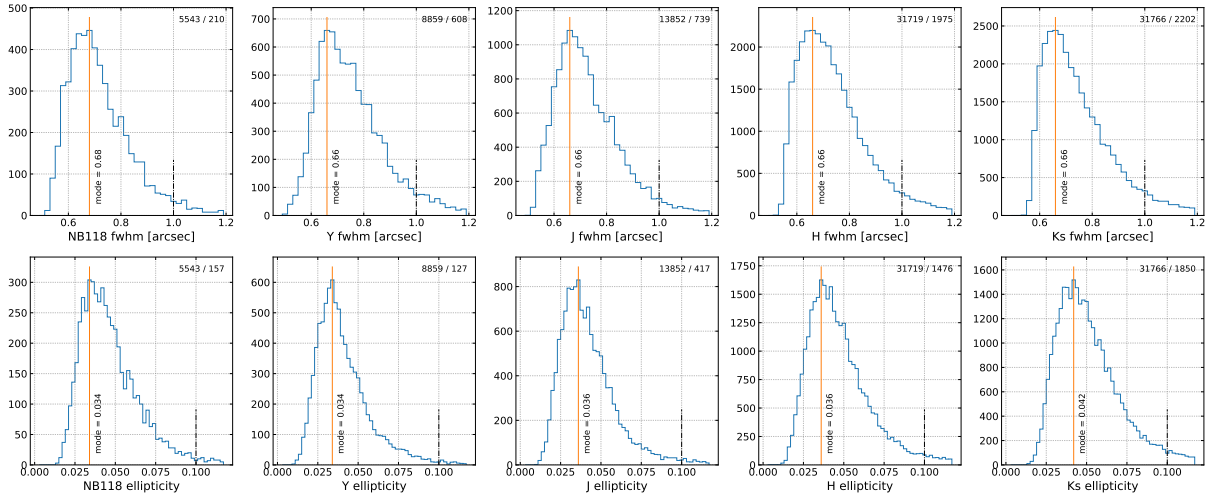


**Figure 1:** FWHM (top) and ellipticity (bottom) distributions for all DR5 images. The red solid line indicates the mode of each distribution, and the blue dashed line shows the cut-off thresholds adopted.

<sup>1</sup><http://casu.ast.cam.ac.uk>

<sup>2</sup><http://casu.ast.cam.ac.uk/surveys-projects/vista/technical/data-processing>

<sup>3</sup>For the sake of good order we will mention a tiny irregularity: Our workflow is that CASU does the basic processing of the individual images (specifically dark correction, nonlinearity correction, and flat field correction). We did indeed select 81,125 of these images for our processing. However, it turned out that the corresponding number of raw images is 29 less, as 29 raw images have accidentally been used twice. This happened because these raw images were processed twice by CASU and somehow given different file names, making us not realise the issue before the stacks had already been made. This is in  $K_s$  ultra-deep where we stack around 10,000 images at each point in the sky. The “duplicate” images only give a *tiny* suboptimal weighting of the underlying data. The duplicate images have not been counted when computing the exposure time in Tab. 3.

## 3 Release Content

### 3.1 Overview

In this release we provide five stacked images and their corresponding weight maps for  $YJHK_s$  and NB118 narrow-band data<sup>4</sup> taken during the first ten years of UltraVISTA survey operations; the new data mainly add exposure time to the “deep” stripes of the  $J$  and  $H$  filters to bring them to nearly the same depth as the “ultra-deep” stripes. In addition, single band individual source lists and source lists created in dual-image mode (using the  $K_s$  image as a detection image) are provided (note that in ESO terminology, single-band tabular data are referred to as “Source lists” and multi-band merged data are referred to as catalogues). We also provide a five-band catalogue that meets the requirement for a catalogue in the Phase 3 framework. The data volume is  $\sim 90$  GB as in DR4.

The total survey area is close to  $1.9 \text{ deg}^2$ . Note that, as in DR4, the “bad” region of detector 16 (having an unstable QE and higher noise) has not been masked.

### 3.2 Special image header contents

The files released follow ESO’s Phase 3 standard for the FITS headers, including the type and form of the provided metadata. As previously, we have made a small extension to this scheme in the form of `COMMENT` FITS header lines to provide additional information related to the particular structure of UltraVISTA. The UltraVISTA field of  $1.5 \text{ deg} \times 1.2 \text{ deg}$  (a VIRCAM tile) does not have a uniform depth; rather the field is covered by 4 *ultra-deep stripes* and 4 *deep stripes*. This is shown in Fig. 1 in McCracken et al. (2012), and it is quantified in the weight maps that are included in this release.

Specifically, we have set the `EXPTIME` keyword (giving the typical exposure time per pixel in seconds), to the value for the ultra-deep stripes. And in `COMMENT` lines we list the value for both sets of stripes, e.g. for the  $K_s$ -band stack:

```
COMMENT ultra-deep stripes: typ. exptime per px = 607980.1 s (keyword EXPTIME)
COMMENT      deep stripes: typ. exptime per px = 499960.0 s
```

Similarly we have set the `ABMAGLIM` keyword (giving the limiting magnitude) to the value for the ultra-deep stripes, and given the value for both sets of stripes in `COMMENT` lines, e.g. for the  $K_s$ -band stack:

```
COMMENT ultra-deep stripes: typical ABMAGLIM = 24.8 (keyword ABMAGLIM)
COMMENT      deep stripes: typical ABMAGLIM = 24.7
```

Finally, we follow the standard and provide keywords `DIT` and `NDIT` keywords only in the stacks where all the individual images had the same value of `DIT` and/or `NDIT`. In all stacks we give the breakdown of number of individual images on the different `DIT`,`NDIT` combinations in `COMMENT` lines, e.g. for the  $K_s$ -band stack:

---

<sup>4</sup>The 16 NB118 filters (one per detector) are described in Milvang-Jensen et al. (2013)

```

COMMENT Breakdown of the used images on different NDIT,DIT combinations
COMMENT N_images NDIT DIT
COMMENT      27696      6    10
COMMENT           25      6     1

```

## 4 Release notes

### 4.1 Data reduction and calibration

All processing was performed on CANDIDE (Computer for Deep Imaging Data for Euclid) cluster of the CALET<sup>5</sup> (Collaboration for wide-field Astronomy Linked to Euclid and other Telescopes) data centre. As the name suggests, this data centre is primarily dedicated to processing associated ground- and space-based data for Euclid and the Euclid calibration fields including UltraVISTA/COSMOS. This new structure ensures that we have support for processing operations well after the completion of UltraVISTA.

In early 2020 we downloaded from CASU<sup>6</sup> all available individual sky-subtracted images covering observing seasons 1–10 (namely 91,731 files covering the period from December 2009 to June 2019 (processed by version 1.3 or 1.5 of the CASU pipeline<sup>7</sup>), the corresponding sky frames (typically one sky frame for each CASU stack covering 0.5–1 h exposure, although two sky frames for NB118 CASU stacks covering 1 h exposure), flat-fields, bad pixel maps and stacked `_st` images. We reprocessed the full dataset so as to take advantage of various improvements in our processing pipeline.

The image files are arranged in OBs (Observation Blocks) of typically 15 or 30 files (@ 2 min exposure) for  $Y$ ,  $J$  and NB118 and 30 or 60 files (@ 1 min exposure) for  $H$  and  $K_s$  (but sometimes just a few files), obtained with the same filter and dithered around one of the “paw” positions. The CASU processing builds a sky image from each OB and subtracts it from each file of the OB. Then the mean value of the subtracted sky is added back to the image (in order to keep noise properties correct).

As in previous releases, the processing begins with an image characterisation step in which the PSF’s FWHM and ellipticity  $e$  are determined and the histogram of valid (not flagged by the bad pixel mask) pixels is computed. While in DR4 and previous releases images with FWHM  $> 1.0''$  or  $e > 0.1$  were rejected before further processing, for this release it was deemed that such images could still be used for determining sky frames, and image rejection was instead done just before the building the final stacks.

In this release we also added a new selection criterion based on the width of the histogram of valid pixels. This method was originally devised to identify files that suffered from a problem in an electronic controller that was reported by ESO in August 2019, and it picks up also other problems with the images. The histogram of valid pixels is used for this purpose. Figure 2 shows that histogram for each chip of a normal and a problem file. The histograms normally show a peak at the typical sky level which is nearly Gaussian near the top with a width determined by the sky noise, and a long tail towards larger values due to the objects detected. A very broad

---

<sup>5</sup><https://calet.org/calet/>

<sup>6</sup><http://casu.ast.cam.ac.uk/vistasp/>

<sup>7</sup><http://casu.ast.cam.ac.uk/surveys-projects/vista/data-processing/version-log>

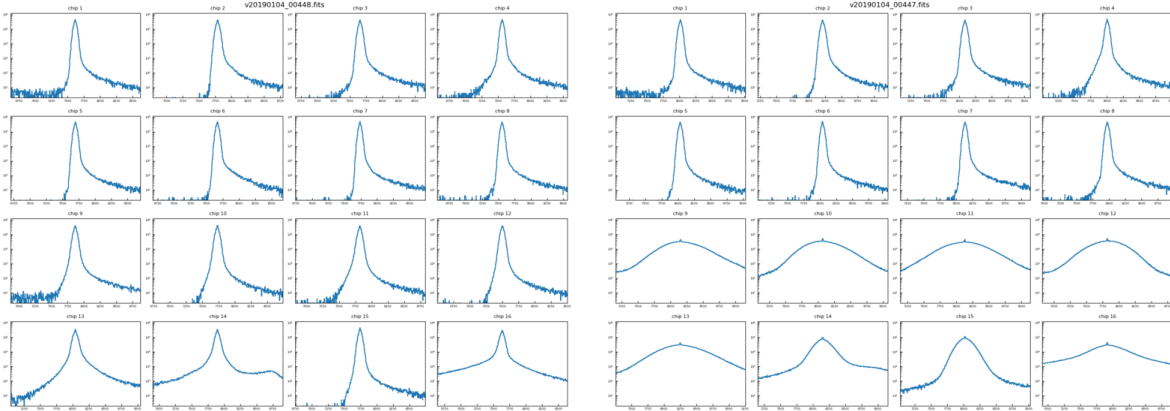


**Figure 2:** Histogram (logarithmic  $y$ -axis) of the values (ADUs) of valid pixels for each of the 16 detector images of a normal and a problem file. Detector images with a problem have very broad histograms.

histogram is a clear indication that something is wrong. So the selection is based on the ratio of height of the peak to its width near the base, and the threshold value is determined empirically.

While previous releases used a *first pass* stack of valid images to produce a *global* mask of objects, in DR5 this mask was built from the DR4 final products. These masks, one per filter, are used to build *local* masks of objects for each input file that include objects much fainter that could be identified in the individual files.

In addition to determining the astrometric correction, here based on the Gaia EDR3 catalogue, **SCAMP** (Bertin 2006) also performs a photometric calibration. While for the astrometric correction each file can be processed individually, for the photometric correction they must be processed together and a reference frame must be established. But because of the large number of files, it is impractical to process them all in a single run of **scamp**, so the **scamp** processing was split into groups of 500 files each. By default **scamp** uses the first frame of group as a photometric reference, and the **FLXSCALE** keyword of all subsequent files are adjusted to be consistent with that frame. But this would yield different calibration among the different groups. Fortunately **scamp** also offers a method of declaring which file or files to use as photometric reference (in practice this is done setting a setting the **PHOTREF** keyword in the file or in an external head file used in input). Our solution was to select all files with FWHM close to the median value as photometric reference files, which ensures that many such files are found in each group. While this is not a guarantee that the exact same reference value is used in all groups, it should ensure a good level of homogeneity.

Prior to determining the sky for each image, the originally subtracted CASU sky is added back in and the constant sky (as given in the **SKYLEVEL** keyword) removed. Then, for each “source” image a sky frame is built from a minimum of 5 and up to 20 other images obtained within 20 min of the “source” image. These images are masked with the source mask derived from the global mask as described above, and median (stack) filtered to produce a source-free image of the sky, which is then subtracted from the “source” image. For a few tens of images (all bands combined) there is not the minimum of 5 nearby images to build a sky frame, and they were rejected.

Finally, destriping (in both  $x$ - and  $y$ - directions) is carried out and large-scale gradients are

removed before re-sampling and re-stacking the images onto the COSMOS astrometric grid, the same that was used in previous releases, for consistency, to produce the final stacks and their respective weight maps. Unlike in previous releases (given the much higher precision of the astrometric solution based on the Gaia EDR3 catalogue), there is no need to build a new astrometric solution for the sky-subtracted images.

It is at this stage, just prior to co-addition, that any file rejection is implemented according to the criteria described earlier.

Co-addition is performed using **SWarp** (Bertin et al. 2002). As in the case of **scamp**, it is impractical to process all files in a single run of **SWarp**. We thus split the full list by paw, then again by season, and then further, if necessary, into equal size groups of less than 500 files. For each sublist the images and weight maps are combined using the “clipped mean stacking” outlier removal technique described in Gruen et al. (2014) with **CLIP\_SIGMA=4.0** in order to build an image substack and its weight map as implemented in **SWarp**. These are built onto the desired our standard COSMOS pixel grid, the same as used previously, with 0.15 arcsec per pixel. Finally, the substacks are merged using a simple weighted average to produce the final full stacks.

## 4.2 Data quality

### 4.2.1 Astrometric accuracy

The astrometric accuracy was measured on the final stacks using catalogues extracted on the stacks and matching them to the Gaia EDR3 reference catalogue. Figure 3 shows the difference between the measured and the reference RA and Dec for all filters. Each plot is roughly the size of an instrumental pixel (0.34 arcsec). And Table 1 lists the mean and FWHM of those distributions, which are about 1/3 of a instrumental pixel.

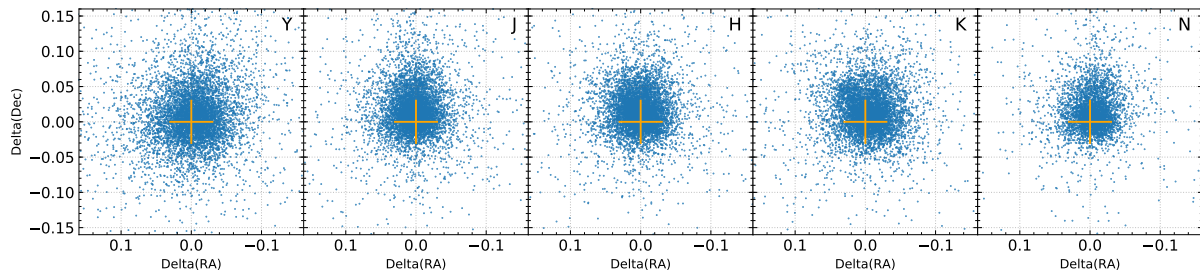


**Figure 3:** The distribution of measured vs reference positions of the astrometric reference sources for all filters. The plot size is roughly one instrument pixel of 0.34 arcsec; in our stacks the pixel size is 0.15 arcsec.

Filter	$\Delta\text{RA}$ [arcsec]		$\Delta\text{Dec}$ [arcsec]	
	mean	FWHM	mean	FWHM
<i>Y</i>	-0.002	0.118	0.011	0.130
<i>J</i>	0.002	0.085	0.017	0.105
<i>H</i>	0.002	0.085	0.015	0.090
<i>K<sub>s</sub></i>	-0.003	0.091	0.014	0.095
NB118	-0.004	0.081	0.017	0.106

**Table 1:** Astrometry accuracy

#### 4.2.2 Comparison of photometry between DR4 and DR5

We also compared the photometry of sources in our DR5 stacks with previous DR4 stacks. Figure 4 shows the difference between `MAG_AUTO` magnitudes measured for all sources in DR4 and in DR5. The small points show one point in fifty. The large points show the median magnitude, and the red lines the region covered by 68% of the points. In all cases, the difference in photometry is less than 0.03 magnitudes.

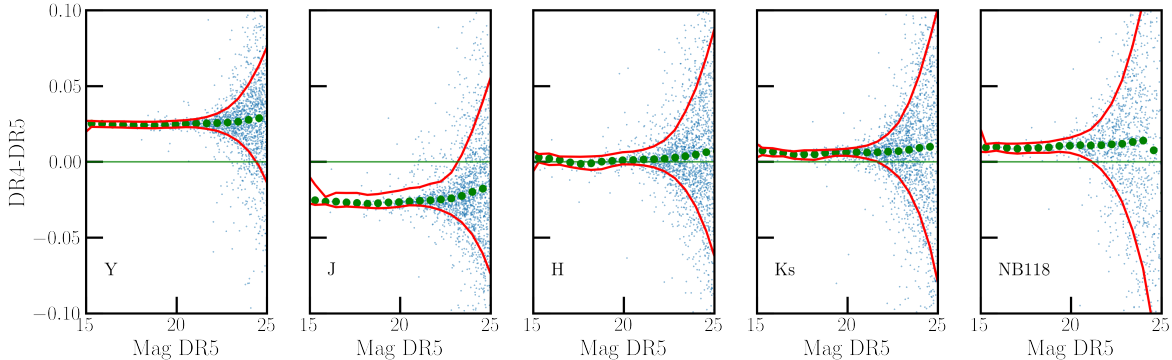


**Figure 4:** Difference in `MAG_AUTO` magnitudes for all sources measured in DR4 and DR5. The filled points show the median values and the solid lines indicate the region covered by 68% of the points.

#### 4.2.3 Limiting magnitudes and seeing

The  $5\sigma$  noise in the stacks in  $2''$  apertures was computed using empty apertures (regions of the images which contained no pixels identified as objects). We computed the noise in the two sets of stripes (deep and ultra-deep), and we also computed the noise in the DR4 stacks in exactly the same way to track the change in depth. The results are given in Table 2. These values represent the  $5\sigma$  noise in  $2''$  apertures — they do not include an aperture correction (of around 0.3 mag, see below) to total magnitude, and in that sense they are not limiting magnitudes. The two sets of stripes have a small overlap on the sky, but for computing the noise reported here we used sufficiently narrow (in RA) definitions of the stripes that this overlap is not used in the analysis. The final column of Table 2 gives the change in noise (and hence change in depth or limiting magnitude) from DR4 to DR5. It can be seen that in the deep stripes in *J* and *H* the depth increased by 0.96 mag, and in *K<sub>s</sub>* by 0.23 mag. The table also shows that in DR5, the

depth across the field is not far from uniform in  $J$ ,  $H$  and  $K_s$ , where the ultra-deep stripes are just 0.18, 0.14 and 0.14 mag (respectively) deeper than the deep stripes.

Filter	Stripes	DR4	DR5	DR5–DR4
$Y$	ultra-deep	26.01	26.02	0.01
$Y$	deep	24.91	24.83	−0.08
$J$	ultra-deep	25.80	25.85	0.05
$J$	deep	24.71	25.67	0.96
$H$	ultra-deep	25.48	25.48	0.00
$H$	deep	24.38	25.34	0.96
$K_s$	ultra-deep	25.12	25.14	0.02
$K_s$	deep	24.77	25.00	0.23
NB118	ultra-deep	24.54	24.64	0.10

**Table 2:** The  $5\sigma$  noise in AB mag in DR4 (for reference) and in DR5, computed in the same way. The final column gives the change in noise (and hence change in depth or limiting magnitude).

For the Phase 3 headers, the limiting magnitude needs to be stated. We computed that by subtracting an approximate aperture correction (from  $2''$  to total magnitude) of 0.3 mag from the  $5\sigma$  noise values reported for DR5 in Tab. 2. These limiting magnitudes are listed in Tab. 3. Table 3 also lists the typical exposure times per pixel, in hours, for the two sets of stripes. These values are calculated as the total time spent on the given set of stripes, multiplied by 2/3, reflecting that a typical point (pixel) on the sky will be covered by 2 of the 3 pawprints that make up a given set of stripes (this is due to the gaps between the detectors of VIRCAM). The PSF FWHM and ellipticity in the stacks (not split by stripes) were measured using PSFEx, and are also listed in Tab. 3.

Filter	Exposure time		Limiting mag.		FWHM	Ellipticity
	per px [hrs]		$5\sigma, 2''$ [AB mag]		[arcsec]	
	Ultra-deep	Deep	Ultra-deep	Deep	Entire image	Entire image
$Y$	167.1	9.9	25.7	24.5	0.77	0.01
$J$	174.6	104.5	25.6	25.4	0.76	0.01
$H$	181.6	125.5	25.2	25.0	0.76	0.01
$K_s$	168.9	138.9	24.8	24.7	0.76	0.01
NB118	119.3	0.0	24.3	N/A	0.75	0.01

**Table 3:** Characteristics of the images: typical exposure time per pixel and limiting magnitudes in both deep and ultra-deep regions and PSF FWHM and ellipticity measured in the entire image. **Important note:** The limiting magnitudes listed in this table and in the headers are computed using “empty aperture” measurements in  $2.0''$  diameter apertures, and are subsequently corrected to total magnitude by subtracting 0.3 mag. This is the same procedure used for DR4.

### 4.3 Known issues

#### 4.3.1 Astrometric accuracy

We note that in determining the astrometric correction, the reference stars were not moved to their position at the time of the UltraVISTA observations. As the epoch of the Gaia EDR3



catalogue is 2016.0, the accuracy varies with time, decreasing from season 1 (2009–2010, FWHM = 0.15 arcsec) to season 7 (2015–2016, FWHM = 0.07 arcsec), then increasing again up to season 10 (2018–2019, FWHM = 0.11 arcsec). Furthermore, since the deep and ultra-deep stripes were observed at different times, the astrometric accuracy can differ between the two. This variation is most important at  $Y$  and at  $K_s$ : at  $Y$  the deep stripes were observed briefly only during season 1, when the dispersion due to the PMs are largest, while the ultra-deep stripes were observed seasons 1–8. At  $K_s$  the deep stripes were also observed briefly in season 1, but then most of the observations come from seasons 6–10, while most of the observations of the ultra-deep stripes were done during the first 5 seasons, thus resulting in a large dispersion. This variation is shown graphically in Figure 5. This issue will be addressed further in the upcoming DR6 and final UltraVISTA data release (planned for early 2024). DR6 will be based on the complete UltraVISTA dataset, from December 2009 to March 2023.

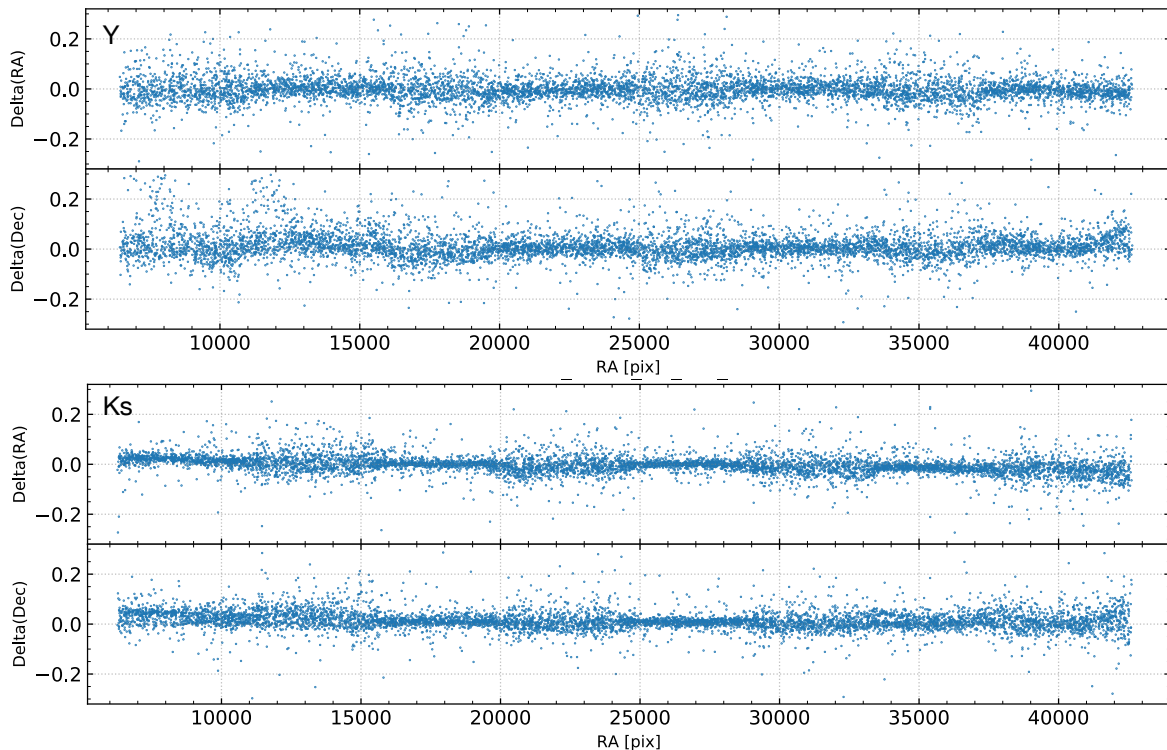


**Figure 5:** The variation of  $\Delta RA$  and  $\Delta Dec$  (arcsec) for the  $Y$  and  $K_s$  observations as a function of RA position in pixels.

A second effect is a slight movement of the centre of the 2D distribution with time, as seen best in  $\Delta RA$  panel for the  $K_s$  filter in Figure 5. Table 4 gives the mean positions and FWHM of the differences, always for  $K_s$ , and Figure 6 shows the 2D plots for all seasons. Keep in mind that the COSMOS field is observable between early November of one year and early July of the following year.

Season	Num	$\Delta\text{RA}$ [arcsec]		$\Delta\text{Dec}$ [arcsec]	
		mean	FWHM	mean	FWHM
2009—10	1	0.013	0.149	-0.008	0.140
2010—11	2	0.015	0.138	-0.009	0.131
2011—12	3	0.012	0.122	-0.014	0.117
2012—13	4	0.008	0.097	-0.015	0.101
2013—14	5	0.004	0.085	-0.015	0.090
2014—15	6	0.001	0.070	-0.013	0.074
2015—16	7	-0.002	0.065	-0.017	0.074
2016—17	8	-0.005	0.072	-0.017	0.079
2017—18	9	-0.008	0.089	-0.018	0.090
2018—19	10	-0.009	0.106	-0.019	0.104

**Table 4:** Astrometry shift and accuracy per observing season for the  $K_s$  band

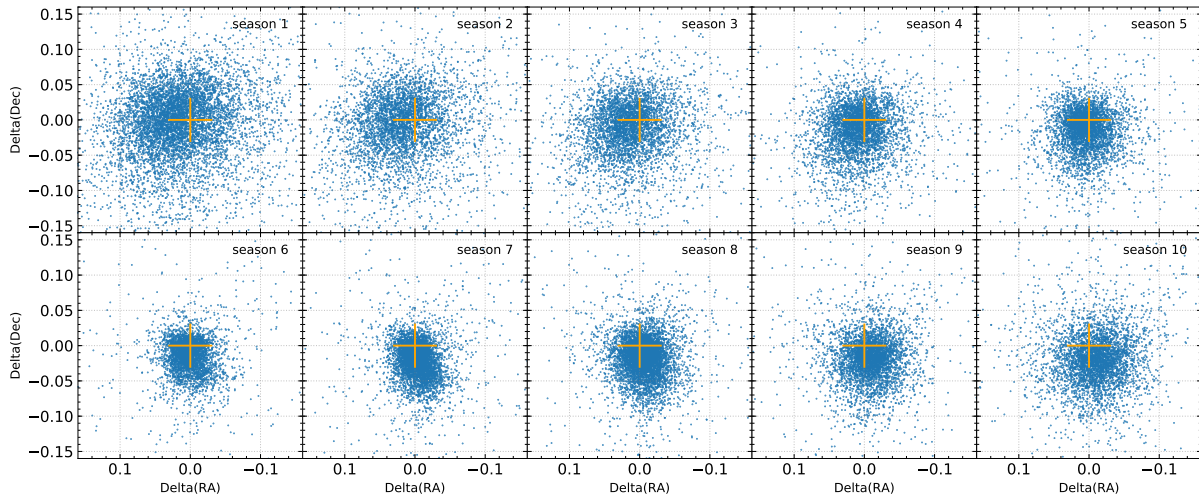


**Figure 6:** The differences between the measured and reference positions, in arcsec, for the  $K_s$  band observations as a function of observing season. The yellow cross gives the origin.

#### 4.4 Previous releases

The science files in DR5 (stacks, sources lists and the 5-band catalogue) supersede – or in the Phase 3 terminology: *update* – the corresponding science files from DR4, which in turn did the same for those in DR3, etc.

The “DR4.1” and “DR4.1.1” releases, which is the Weaver et al. (2022) COSMOS2020 multi-band (ca. 40 bands) catalogues based on the UltraVISTA DR4 images and other data (UV, optical, IR, ...), are not “superseded” (updated) by this DR5 release, as it does not contain such  $\sim 40$ -band catalogues (only a 5-band catalogue based on the UltraVISTA data alone). For information: DR4.1 was the initial release of the two COSMOS2020 catalogues, called Classic and Farmer. DR4.1.1 contains an updated version of the Farmer catalogue where a minor error has been corrected.

## 4.5 Software versions

DR5 makes extensive use of the `Astromatic`<sup>8</sup> software. A complete list of software versions used is listed in Table 5.

Software name	Version
<code>SExtractor</code>	2.24.2
<code>PSFEx</code>	3.22.1
<code>Scamp</code>	2.10.0
<code>SWarp</code>	2.41.5
<code>WeightWatcher</code>	1.12
<code>MissFITS</code>	2.8.0

**Table 5:** Software versions used in UltraVISTA DR5.

## 5 Data format

### 5.1 File types

All images and catalogues are distributed in FITS format. In this release, we provide five stacked images and their corresponding weight maps for  $Y$ ,  $J$ ,  $H$ ,  $K_s$ , and NB118 narrow-band data composed of images from the first ten years of the UltraVISTA public survey.

Given the deep and ultra-deep sections have different exposure times, this has the important consequence that the signal-to-noise ratio for an object of a given magnitude will vary across the image. An inspection of the weight map provided with each image will indicate the location of the deeper zones.

Images have a zero-point of 30.0 AB magnitudes for a one second equivalent exposure time. The images have a pixel scale of  $0.15''/\text{pixel}$  and have the same pixel grid (number of pixels and tangent point) as the other publicly available IRSA/COSMOS images. Each image is  $\sim 9$  GB in size.

Following the ESO Phase 3 standard, the FITS files for the 5 stacks are multi-extension FITS files, with the stacked image in the primary HDU (header data unit) and with a “provenance table” in the first (and only) extension. The provenance table lists all the raw images that (after processing at CASU and CALET) were combined to make the given stack. The provenance table for a image stack applies also to its weight map and is not repeated there.

### 5.2 Complete list of distributed products

Tables 6 and 7 list the imaging, source list and catalogue data products distributed in DR5. Five images are provided, as well as their corresponding weight maps. These weight-maps correspond to the `MAP_WEIGHT` images produced by `SWarp` and have pixel values proportional to the inverse variance. We note that we plan to put all the 20 DR5 files on our website<sup>9</sup>.

---

<sup>8</sup><https://www.astromatic.net/>

<sup>9</sup><http://www.ultravista.org/>

Filename	Description
UVISTA_Y_12_07_22_allpaw_skysub_015_dr5_rc_v1.fits	Y-band stack
UVISTA_Y_12_07_22_allpaw_skysub_015_dr5_rc_v1.weight.fits	Y-band weight
UVISTA_J_12_07_22_allpaw_skysub_015_dr5_rc_v1.fits	J-band stack
UVISTA_J_12_07_22_allpaw_skysub_015_dr5_rc_v1.weight.fits	J-band weight
UVISTA_H_12_07_22_allpaw_skysub_015_dr5_rc_v1.fits	H-band stack
UVISTA_H_12_07_22_allpaw_skysub_015_dr5_rc_v1.weight.fits	H-band weight
UVISTA_Ks_12_07_22_allpaw_skysub_015_dr5_rc_v1.fits	Ks-band stack
UVISTA_Ks_12_07_22_allpaw_skysub_015_dr5_rc_v1.weight.fits	Ks-band weight
UVISTA_NB118_12_07_22_allpaw_skysub_015_dr5_rc_v1.fits	NB118-band stack
UVISTA_NB118_12_07_22_allpaw_skysub_015_dr5_rc_v1.weight.fits	NB118-band weight

**Table 6:** Summary of DR5 stacked images and associated weight maps. All images have a zero point of 30.0 AB magnitudes for a one second equivalent exposure time and a scale of  $0.15''/\text{pixel}$ .

Filename	Detection	Measurement
UVISTA_Y_12_07_22_allpaw_skysub_015_dr5_rc_v1.cat.fits	<i>Y</i>	<i>Y</i>
UVISTA_J_12_07_22_allpaw_skysub_015_dr5_rc_v1.cat.fits	<i>J</i>	<i>J</i>
UVISTA_H_12_07_22_allpaw_skysub_015_dr5_rc_v1.cat.fits	<i>H</i>	<i>H</i>
UVISTA_Ks_12_07_22_allpaw_skysub_015_dr5_rc_v1.cat.fits	<i>K<sub>s</sub></i>	<i>K<sub>s</sub></i>
UVISTA_NB118_12_07_22_allpaw_skysub_015_dr5_rc_v1.cat.fits	NB118	NB118
UVISTA_Ks_12_07_22_allpaw_skysub_015_dr5_rc_v1_Y.cat.fits	<i>K<sub>s</sub></i>	<i>Y</i>
UVISTA_Ks_12_07_22_allpaw_skysub_015_dr5_rc_v1_J.cat.fits	<i>K<sub>s</sub></i>	<i>J</i>
UVISTA_Ks_12_07_22_allpaw_skysub_015_dr5_rc_v1_H.cat.fits	<i>K<sub>s</sub></i>	<i>H</i>
UVISTA_Ks_12_07_22_allpaw_skysub_015_dr5_rc_v1_NB118.cat.fits	<i>K<sub>s</sub></i>	NB118
UVISTA_5band_cat_dr5_rc_v1.fits	<i>K<sub>s</sub></i>	<i>YJHK<sub>s</sub>NB118</i>

**Table 7:** Source lists and catalogue products delivered with DR5.

We provide two source lists for each band: a “dual-image mode” list, in which the  $K_s$  image is used for source detection and the band image is used as the measurement (i.e., the measurement is done at the position of the source in the  $K_s$  band); and a “single-image mode” list in which the image is used for both detection and measurement. Dual-image mode source lists have the advantage that, as the same number of entries is present in all source lists, colours can be easily computed for each object. On the other hand, the single-image mode lists contain, in principle, all sources to a given detection threshold ( $1.8\sigma$ ). Source lists were extracted using **SExtractor** (Bertin & Arnouts 1996) version 2.24.2 compiled and downloaded from the [astromatic.net](http://astromatic.net)<sup>10</sup>. For each entry in the source list we provide flux measurements in 18 photometric apertures. Their diameters in pixels ( $1 \text{ px} = 0.15''$ ) are as follows, corresponding to three apertures of  $2''$ ,  $3''$  and  $7.1''$  and logarithmically spaced apertures from  $0.5''$  to  $5''$ :

13.33, 20.00, 47.33,  
3.33, 3.93, 4.63, 5.46, 6.44, 7.59, 8.94, 10.54, 12.43, 14.65, 17.26, 20.35, 23.99, 28.28, 33.33

We also provide a 5-band catalogue `UVISTA_5band_cat_dr5_rc_v1.fits` created from the five  $K_s$ -selected source lists. The columns in this catalogue are described in Tab. 8. Two additional columns are provided: the  $E(B - V)$  Galactic reddening measured at the position of each object in the Schlegel et al. (1998) dust maps, and a flag which indicates the field border.

<sup>10</sup><http://astromatic.net/software/sextractor>

Column no.	Column name	Description
1	SOURCE_ID	UltraVISTA source designation (DR5)
2	NUMBER	Running object number
3	ALPHA_J2000	Right ascension of barycenter in decimal degrees (J2000)
4	DELTA_J2000	Declination of barycenter in decimal degrees (J2000)
5	X_IMAGE	Object position along x
6	Y_IMAGE	Object position along y
7	FLAG_HJMCC	Bad region flag: != 0 for bad region (field boundaries: 1)
8	EBV	Galactic reddening E(B-V) based on Schlegel et al (1998) dust maps
9	Y_APER2	Y fixed aperture magnitude (2")
10	Y_APER2_ERR	Y fixed aperture mag error (2")
11	Y_APER7	Y fixed aperture magnitude (7.1")
12	Y_APER7_ERR	Y fixed aperture mag error (7.1")
13	Y_AUTO	Y auto magnitude
14	Y_AUTO_ERR	Y auto mag error
15	Y_FLUX_RADIUS	Radius of aperture containing half the flux of Y_AUTO
16	Y_FLAG	Y Flag (SExtractor)
17	J_APER2	J fixed aperture magnitude (2")
18	J_APER2_ERR	J fixed aperture mag error (2")
19	J_APER7	J fixed aperture magnitude (7.1")
20	J_APER7_ERR	J fixed aperture mag error (7.1")
21	J_AUTO	J auto magnitude
22	J_AUTO_ERR	J auto mag error
23	J_FLUX_RADIUS	Radius of aperture containing half the flux of J_AUTO
24	J_FLAG	J Flag (SExtractor)
25	H_APER2	H fixed aperture magnitude (2")
26	H_APER2_ERR	H fixed aperture mag error (2")
27	H_APER7	H fixed aperture magnitude (7.1")
28	H_APER7_ERR	H fixed aperture mag error (7.1")
29	H_AUTO	H auto magnitude
30	H_AUTO_ERR	H auto mag error
31	H_FLUX_RADIUS	Radius of aperture containing half the flux of H_AUTO
32	H_FLAG	H Flag (SExtractor)
33	KS_APER2	Ks fixed aperture magnitude (2") [detection image]
34	KS_APER2_ERR	Ks fixed aperture mag error (2") [detection image]
35	KS_APER7	Ks fixed aperture magnitude (7.1") [detection image]
36	KS_APER7_ERR	Ks fixed aperture mag error (7.1") [detection image]
37	KS_AUTO	Ks auto magnitude [detection image]
38	KS_AUTO_ERR	Ks auto mag error [detection image]
39	KS_FLUX_RADIUS	Radius of aperture containing half the flux of KS_AUTO
40	KS_FLAG	Ks Flag (SExtractor) [detection image]
41	NB118_APER2	NB118 fixed aperture magnitude
42	NB118_APER2_ERR	NB118 fixed aperture mag error
43	NB118_APER7	NB118 fixed aperture magnitude
44	NB118_APER7_ERR	NB118 fixed aperture mag error
45	NB118_AUTO	NB118 auto magnitude
46	NB118_AUTO_ERR	NB118 auto mag error
47	NB118_FLUX_RADIUS	Radius of aperture containing half the flux of NB118_AUTO
48	NB118_FLAG	NB118 Flag (SExtractor)

**Table 8:** List of columns in the five-band merged catalogue. All magnitudes are in the AB system.

## 6 Release of the CASU single OB pawprint stacks at VSA/WFAU

As part of the VISTA Data Flow System (e.g. Emerson et al. 2004), CASU produces stacks of the data contained in a single OB and on a single pawprint (e.g. Irwin et al. 2004; Lewis et al. 2010, and the CASU web site<sup>11</sup>). These stacks have `_st` in the file names and are sometimes called `_st` stacks. The UltraVISTA OBs typically comprise 0.5 or 1 hour exposure on a given pawprint, and in UltraVISTA we have somewhat imprecisely referred to these CASU stacks as the “1-hour stacks”. Throughout the UltraVISTA program we have supplied these stacks to interested parties on a best-effort basis. To make these data more widely available we are, since DR4, releasing these stacks through the VISTA Science Archive (VSA, e.g. Hambly et al. 2004; Cross et al. 2012) at the Wide Field Astronomy Unit (WFAU) at Edinburgh, concurrent with the ESO data release of our deep stacks.

It should be noted that our deep stacks are made by redoing the sky subtraction of the individual images corresponding to 1 or 2 minutes of exposure and then stacking these; our deep stacks are not made by stacking the CASU `_st` stacks. We have not used the CASU stacks in our processing, and we are providing them via the VSA “as is”.

The VSA will not only allow the user to download selected or all of the CASU stacks and their confidence maps, it will also allow the user to upload a text file with coordinates of one or more objects, and then in a second step get the photometry from each CASU stack, giving a table including aperture-corrected magnitude and time (MJDOBS), from which a light curve in the five UltraVISTA bands can be plotted.

### 6.1 The CASU single OB pawprint stacks at the VSA

#### 6.1.1 Cookbook: How to download the CASU single OB pawprint stacks and their confidence maps

Go to the VSA (VISTA Science Archive) home page <http://surveys.roe.ac.uk/vsa>

There is no need to login

Click “Archive Listing”

Under “Select the programme/survey you wish to use:” select “UltraVISTA”

Under “Database release to use:” select “ULTRAVISTADR5”

Under “Observation type:” leave it at “object”

Under “Frame type:” select “stack (pawprint)”

Possibly limit by filter or time period

Possibly increase “Rows per page:” up to a max of 1000

Click GetList

Then download the CASU single OB pawprint stacks via the “Link to image wget script” link

To get the CASU confidence maps for these stacks, in the form do:

Under “Observation type:” select “confidence”

Under “Frame type:” select “stack (pawprint)” (as before)

---

<sup>11</sup><http://casu.ast.cam.ac.uk/surveys-projects/vista/technical/data-processing>

## 7 Acknowledgements

This UltraVISTA release has been made possible thanks to a significant infrastructure grant from “Domaine d’intérêt majeur en astrophysique et conditions d’apparition de la vie (DIM-ACAV+)”. HJMCC acknowledges financial support from the “Programme national cosmologie et galaxies” (PNCG). JSD acknowledges the support of the UK Science and Technology Facilities Council (STFC) and the support of the Royal Society through a Research Professorship. The Cosmic Dawn Center is funded by the Danish National Research Foundation under grant no. 140. The UltraVISTA team would like to thank the ESO staff for scheduling and making the UltraVISTA observations. We thank E. Bertin for many useful discussions concerning the usage of the *Astromatic* tool set. This research has made use of the *VizieR* catalogue access tool provided by the CDS, Strasbourg, France. This work has made use of data from the European Space Agency (ESA) mission *Gaia* (<https://www.cosmos.esa.int/gaia>), processed by the *Gaia* Data Processing and Analysis Consortium (DPAC, <https://www.cosmos.esa.int/web/gaia/dpac/consortium>). Funding for the DPAC has been provided by national institutions, in particular the institutions participating in the *Gaia* Multilateral Agreement.

## References

- Bertin, E. 2006, in *Astronomical Society of the Pacific Conference Series*, Vol. 351, *Astronomical Data Analysis Software and Systems XV*, ed. C. Gabriel, C. Arviset, D. Ponz, & S. Enrique, 112
- Bertin, E. 2011, in *Astronomical Society of the Pacific Conference Series*, Vol. 442, *Astronomical Data Analysis Software and Systems XX*, ed. I. N. Evans, A. Accomazzi, D. J. Mink, & A. H. Rots, 435
- Bertin, E. & Arnouts, S. 1996, *ApJS*, 117, 393
- Bertin, E., Mellier, Y., Radovich, M., et al. 2002, in *Astronomical Society of the Pacific Conference Series*, Vol. 281, *Astronomical Data Analysis Software and Systems XI*, ed. D. A. Bohlender, D. Durand, & T. H. Handley, 228
- Cross, N. J. G., Collins, R. S., Mann, R. G., et al. 2012, *A&A*, 548, A119
- Emerson, J. P., Irwin, M. J., Lewis, J., et al. 2004, in *Society of Photo-Optical Instrumentation Engineers (SPIE) Conference Series*, Vol. 5493, *Society of Photo-Optical Instrumentation Engineers (SPIE) Conference Series*, ed. P. J. Quinn & A. Bridger, 401–410
- Gaia* Collaboration, Brown, A. G. A., Vallenari, A., et al. 2021, *A&A*, 649, A1
- Gaia* Collaboration, Prusti, T., de Bruijne, J. H. J., et al. 2016, *A&A*, 595, A1
- Gruen, D., Seitz, S., & Bernstein, G. M. 2014, *Publications of the Astronomical Society of the Pacific*, 126, 158
- Hambly, N. C., Mann, R. G., Bond, I., et al. 2004, in *Society of Photo-Optical Instrumentation Engineers (SPIE) Conference Series*, Vol. 5493, *Society of Photo-Optical Instrumentation Engineers (SPIE) Conference Series*, ed. P. J. Quinn & A. Bridger, 423–431

- Irwin, M. J., Lewis, J., Hodgkin, S., et al. 2004, in Society of Photo-Optical Instrumentation Engineers (SPIE) Conference Series, Vol. 5493, Society of Photo-Optical Instrumentation Engineers (SPIE) Conference Series, ed. P. J. Quinn & A. Bridger, 411–422
- Lewis, J. R., Irwin, M., & Bunclark, P. 2010, in Astronomical Society of the Pacific Conference Series, Vol. 434, Astronomical Data Analysis Software and Systems XIX, ed. Y. Mizumoto, K.-I. Morita, & M. Ohishi, 91
- Lindegren, L., Klioner, S. A., Hernández, J., et al. 2021, A&A, 649, A2
- McCracken, H. J., Milvang-Jensen, B., Dunlop, J., et al. 2012, A&A, 544, A156
- Milvang-Jensen, B., Freudling, W., Zabl, J., et al. 2013, A&A, 560, A94
- Schlegel, D. J., Finkbeiner, D. P., & Davis, M. 1998, ApJ, 500, 525
- Scoville, N., Aussel, H., Brusa, M., et al. 2007, ApJS, 172, 1
- Weaver, J. R., Kauffmann, O. B., Ilbert, O., et al. 2022, ApJS, 258, 11